The magnetic properties of gadolinium/holmium superlattices

1997 J. Phys.: Condens. Matter 9 8727

(http://iopscience.iop.org/0953-8984/9/41/017)

J. Phys.: Condens. Matter **9** (1997) 8727–8735. Printed in the UK PII: S0953-8984(97)85231-9

The magnetic properties of gadolinium/holmium superlattices

C Bryn-Jacobsen†, D F McMorrow‡, R C C Ward† and M R Wells†

† Oxford Physics, Clarendon Laboratory, Parks Road, Oxford OX1 3PU, UK

‡ Condensed Matter Physics and Chemistry Department, Risø National Laboratory, DK-4000, Roskilde, Denmark

Received 23 June 1997

Abstract. The magnetic properties of Gd/Ho superlattices have been investigated using neutron-diffraction techniques. Between $T \approx 297$ K and $T \approx 138$ K, the magnetic moments in each Gd block order ferromagnetically in the basal plane with the moments in adjacent Gd blocks antiferromagnetically aligned. At temperatures below $T \approx 138$ K, the Ho moments order in a basal-plane helix, while the Gd moments remain ferromagnetically aligned in the basal plane with an alignment between adjacent Gd blocks that is dependent on temperature and the Ho-block thickness. The coherence lengths of the magnetic structures in the growth direction range from 350 Å to 800 Å. Comparisons are made with the results from previous studies of heavy rare-earth superlattices.

1. Introduction

Investigations of the magnetic properties of rare-earth superlattices contribute to our understanding of the fundamental interactions in rare-earth metals [1]. Superlattice combinations including the heavy rare-earth elements Gd and Ho have played an important rôle throughout the development of these investigations [2, 3]. Early experiments concentrated on combinations of magnetic and nonmagnetic heavy rare earths, with the results from, for instance, Gd/Y [4] encouraging the development of models for the interlayer coupling (such as the independent-block model [5]) that were based on conventional Ruderman–Kasuya–Kittel–Yosida (RKKY) interactions. More recently these studies have been extended to magnetic/magnetic systems, with superlattices such as Gd/Dy [6] and Ho/Er [7] being among the first to be examined. It is most notably the results from some of these double-magnetic combinations that have questioned the need to refine the original models. For example, it has been suggested that in order to explain the suppression of the ferromagnetic phase of bulk Dy in Dy/Ho [8], it may be necessary to take account of the band structure of the whole superlattice, rather than of the constituent individual blocks. Similarly, the results from a study of Tb/Ho [9] superlattices emphasize the need to consider *in detail* the influence of crystal-field and dipolar interactions in addition to RKKY interactions when considering the possible mechanisms for the interlayer coupling.

Here we present an investigation of Gd/Ho superlattices grown by molecular-beam epitaxy (MBE). Gd and Ho adopt the hexagonal close-packed (hcp) crystal structure, with a mismatch in lattice parameters of less than 2% [10]. The magnetic properties of Gd [11, 12] and Ho [13] have been studied extensively. The magnetic moments in Gd order ferromagnetically at $T_C(\mathrm{Gd}) \approx 292$ K. Despite Gd ions being in *S*-states (i.e. having

0953-8984/97/418727+09$19.50

zero orbital-angular momentum), there is a small residual magnetic anisotropy that favours an alignment of the magnetic moments along the c-axis. At lower temperatures, the moments tilt towards the basal plane, reaching a maximum tilt of 60° at $T \approx 180$ K, before decreasing to just below 30° at $T \approx 4$ K. The magnetic moments of bulk Ho align in a basal-plane helix below $T_N(\mathrm{Ho}) \approx 132$ K. The helical wave vector, $\boldsymbol{q}$, decreases on cooling from $\boldsymbol{q} = 0.275\boldsymbol{c}^*$ to $\boldsymbol{q} = (1/6)\boldsymbol{c}^*$ at $T \approx 18$ K, below which temperature the moments tilt out of the basal plane to form a ferromagnetic cone structure.

2. Experimental techniques

The Gd/Ho superlattices were grown by MBE at the Clarendon Laboratory, Oxford, using the growth techniques described by Ward and Wells [14]. A cleaned sapphire substrate was used for each sample, on which was deposited 1500 Å of Nb as a chemical buffer, and 1800 Å of Y to act as a seed in preparation for the growth of the superlattice layers. With the substrate temperature held at 400 °C, n_{Gd} layers of Gd followed by n_{Ho} layers of Ho were then deposited on the Y seed by evaporating Gd from an electron-beam source and Ho from a Knudsen effusion cell at a rate of 0.5 Å s^{-1}, forming a single bilayer. This bilayer unit was repeated sixty times, and capped with 250 Å of Y to inhibit oxidation of the superlattice. The epitaxial relationships in the growth direction are $\{110\}\mathrm{Al_2O_3} \parallel \{110\}\mathrm{Nb} \parallel \{001\}$Y, Gd/Ho; and the nominal compositions of the samples investigated are $\mathrm{Gd_{10}/Ho_{30}}$, $\mathrm{Gd_{20}/Ho_{20}}$, and $\mathrm{Gd_{30}/Ho_{10}}$ (where the subscripts refer to the number of planes of each element in a single bilayer).

The samples were first examined at $T = 300$ K using a high-resolution triple-axis x-ray diffractometer at the Clarendon Laboratory, Oxford. Scans were performed with the wave-vector transfer along the $[00\ell]$ and $[10\ell]$ directions in reciprocal space, together with transverse scans through the main (002) nuclear Bragg peaks. The samples were subsequently investigated by neutron-diffraction techniques using the triple-axis spectrometer, TAS 1, situated on the cold source of the DR3 reactor at the Risø National Laboratory. Neutrons of energy 5 meV were selected using pyrolytic-graphite monochromator and analyser crystals, with higher-order contamination reduced by a cooled beryllium filter. The samples were mounted in a closed-cycle cryostat with the $(h0\ell)$ plane in the scattering plane. The reactor-to-sample collimations of 120′–30′–60′–140′ resulted in a wave-vector resolution in the scattering plane of approximately 0.012 $\mathrm{Å}^{-1}$ (full width at half maximum (FWHM)). At selected temperatures between $T = 300$ and 12 ± 1 K, scans were performed with the wave-vector transfer along $[00\ell]$ (to investigate the ordering of moments in the basal plane) and along $[10\ell]$ (to additionally obtain information about components of ordered moments along the c-axis).

3. Analysis

The FWHM in reciprocal space, ΔQ, of the nuclear Bragg peaks measured with x-rays were used to deduce real-space structural coherence lengths, ξ, using the relationship $\xi = 2\pi/\Delta Q$; with the FWHM of peaks along $[00\ell]$ yielding the coherence of the stacking of close-packed planes in the growth direction, and the FWHM of scans along $[10\ell]$ indicating the coherence of the hcp stacking sequence. The FWHM of transverse scans through the main (002) Bragg peaks give the mosaic-spread values of the samples. The nominal bilayer compositions were refined by fitting independently models of the superlattice structure described by Bryn-Jacobsen *et al* [15] to the scattering measured from scans of

the wave-vector transfer along $[00\ell]$ at $T = 300$ K using x-rays and neutrons.

In order to study only the neutron *magnetic* scattering from the samples, the neutron structural scattering measured at $T = 300$ K (a temperature above the highest magnetic-ordering temperature) was subtracted from the total neutron scattering measured at each temperature. This approach assumes a negligible change with temperature of the structural scattering from the superlattice layers, as was confirmed for scattering from Tb/Ho [9] layers using x-ray scattering techniques. The subtraction for Gd/Ho yields a generally smooth variation of intensity with wave vector, and the results are always positive indicating that they are not significantly affected by any changes in the structural scattering from the Gd/Ho layers, or from the Y seed and cap.

At each temperature measured, a model simulating the scattering from a magnetic structure was fitted simultaneously to the magnetic-scattering results obtained from scans of the wave-vector transfer along $[00\ell]$ and $[10\ell]$. The model is based on that developed by Jehan *et al* [16] and adapted by Bryn-Jacobsen *et al* [9] for the analysis of the predominantly ferromagnetic/helical system, Tb/Ho. Hyperbolic tangent functions are used to include the variations in the structural and magnetic properties owing to the widths of the interfaces. Guided by the magnetic ordering of the bulk elements and of Tb/Ho superlattices, the model chosen simulates the magnetic scattering from a basal-plane ferromagnetic ordering of Gd moments and a basal-plane helical ordering of Ho moments.

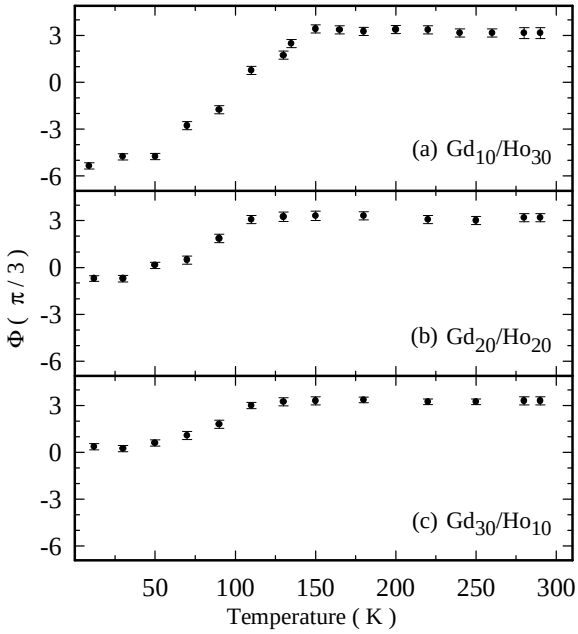

Figure 1. The temperature dependence of the total turn angle per bilayer, Φ (modulo 2π), for (a) Gd_{10}/Ho_{30}, (b) Gd_{20}/Ho_{20}, and (c) Gd_{30}/Ho_{10} determined from the offset of the neutron structural and magnetic scattering as described in section 3.

To obtain initial values for the turn angle per plane in the Ho layers, ϕ_{Ho}, the offset in the positions of the peaks in the magnetic scattering from the positions of the nuclear Bragg peaks at $T = 300$ K was used [9] to calculate the total turn angle per bilayer, Φ (modulo 2π) shown in figure 1. Assuming a ferromagnetic ordering of Gd moments, ϕ_{Ho} was then

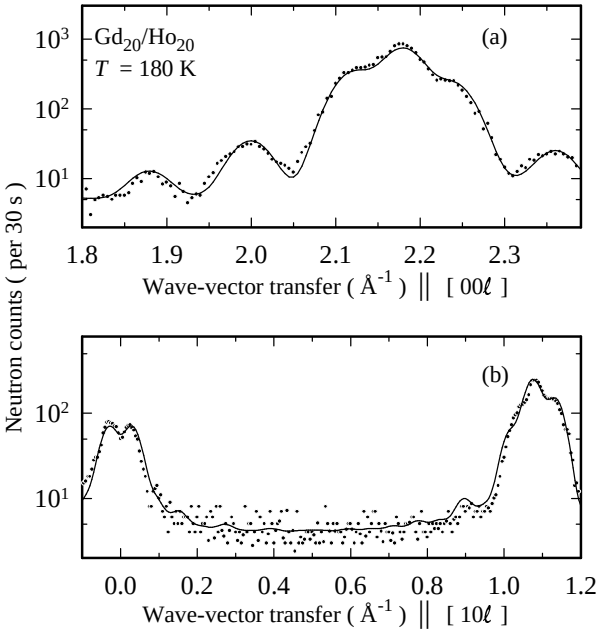

Figure 2. The solid points show the magnetic-scattering results for Gd_{20}/Ho_{20} at $T = 180$ K from scans of the wave-vector transfer along (a) [00ℓ], and (b) [10ℓ]. The solid lines are a fit to the data using a model that calculates the magnetic scattering from a basal-plane ferromagnetic ordering of Gd moments, and a phase advance over the Ho layers which are not magnetically ordered.

Table 1. The structural characteristics of the samples deduced from x-ray measurements at $T = 300$ K as described in section 3. The [00ℓ] and [10ℓ] coherence lengths indicate long-range coherence of the stacking of close-packed planes in the growth direction, and of the hcp stacking sequence, respectively; while the small mosaic-spread values reflect good sample crystallinity.

Nominal composition	Fitted composition (±1 plane)	[00ℓ] coherence length (±150 Å)	[10ℓ] coherence length (±250 Å)	Mosaic (±0.03°)
Gd_{10}/Ho_{30}	$Gd_{10.5}/Ho_{28.0}$	3300	1100	0.12
Gd_{20}/Ho_{20}	$Gd_{19.0}/Ho_{18.0}$	2800	1000	0.14
Gd_{30}/Ho_{10}	$Gd_{31.0}/Ho_{9.5}$	3600	1200	0.11

calculated from Φ (modulo 2π) by dividing by the fitted values of n_{Ho} (table 1).

Finally, estimates were made for each sample of the magnitude of the ordered Gd and Ho moments at $T = 12$ K by comparing the intensity at $T = 300$ K of the neutron nuclear scattering at (002), with the intensity at $T = 12$ K of the neutron magnetic scattering [17].

4. Results

As summarized in table 1, long-range coherence lengths are found for the stacking of close-packed planes in the growth direction (over 2500 Å), and for the hcp stacking sequence (typically 1000 Å). In addition, the relatively [15] small mosaic-spread values of

Table 2. The lattice parameters a are those measured at $T = 300$ K using neutrons. T_C(Gd) and T_N(Ho) are the ordering temperatures of the Gd and Ho moments, respectively. The magnitudes of the ordered Gd and Ho moments, m(Gd) and m(Ho), respectively, are for $T = 12$ K and were calculated as described in section 3.

Nominal composition	a (± 0.002 Å)	T_C(Gd) (± 2 K)	T_N(Ho) (± 2 K)	m(Gd) $\pm 1\mu_B$	m(Ho) $\pm 1\mu_B$
Gd_{10}/Ho_{30}	3.606	296	139	6.9	8.6
Gd_{20}/Ho_{20}	3.613	297	138	7.0	8.8
Gd_{30}/Ho_{10}	3.624	297	138	6.7	8.3

approximately 0.15° indicate good sample crystallinity. The results for the fitted bilayer compositions using x-ray and neutron measurements are the same within error, with a comparison of the more accurate values obtained using x-ray measurements with the nominal bilayer compositions given in table 1.

The magnetic-structure model gives good fits to the magnetic-scattering results, with interface widths of 3 ± 1 planes. After allowing for the differences in structure factors, the scale factors required to fit the magnetic-scattering results from scans of the wave-vector transfer along $[00\ell]$ and $[10\ell]$ differ by less than 5% at all temperatures measured. Given that the model assumes a basal-plane ordering of Gd and Ho moments, this equality of scale factors indicates that the Gd and Ho moments are confined to the basal plane.

Between $T \approx 297$ K and $T \approx 138$ K, the fits of the model to the magnetic scattering

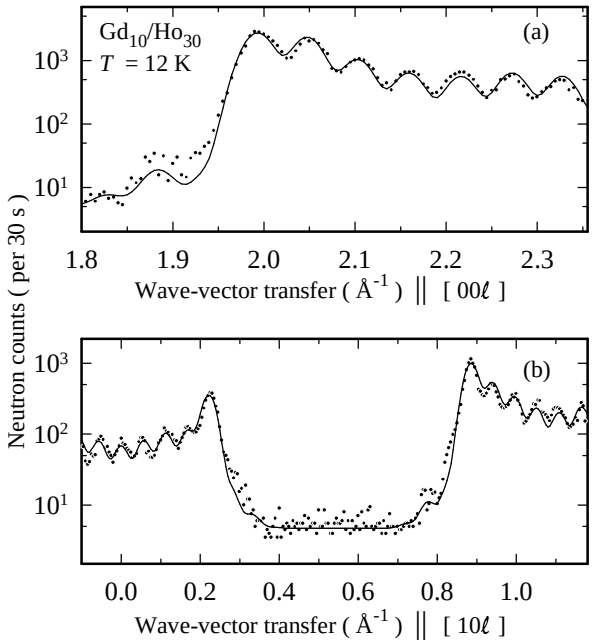

Figure 3. The solid points show the magnetic-scattering results for Gd_{10}/Ho_{30} at $T = 12$ K from scans of the wave-vector transfer along (a) $[00\ell]$, and (b) $[10\ell]$. The solid lines are a fit to the data of a model that simulates the magnetic scattering from a basal-plane ferromagnetic ordering of Gd moments, and basal-plane helical ordering of Ho moments.

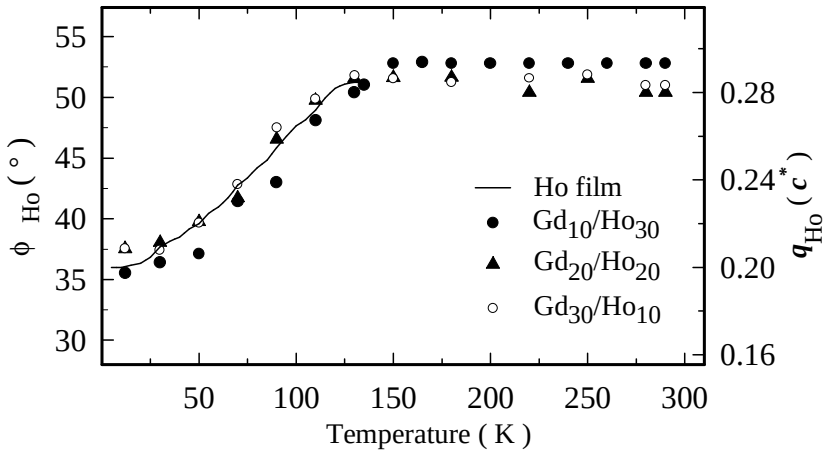

Figure 4. The turn angles per plane in the Ho layers, $\phi_{\mathrm{Ho}} \pm 1^\circ$ ($\boldsymbol{q}_{\mathrm{Ho}}$), for the Gd/Ho superlattices compared to a 5000 Å film of Ho grown on an Y seed [19].

indicate a basal-plane ferromagnetic alignment of Gd moments within Gd blocks, and a phase advance over the Ho blocks within which the Ho moments are not magnetically ordered. Estimates of the temperature for each sample of the onset of ordering in the Gd blocks, T_{C}(Gd), were deduced from the temperature dependences of the total magnetic scattering above $T = 138$ K, and are listed in table 2. Figure 2 illustrates a fit of the model to the magnetic scattering from Gd_{20}/Ho_{20} at $T = 180$ K.

For $T \lesssim 138$ K, the fits of the model to the magnetic scattering indicate that in addition to the basal-plane ferromagnetic ordering of Gd moments within Gd blocks, there is a basal-plane helical ordering of the Ho moments within the Ho blocks. For each sample, the temperature at which the Ho moments order, T_{N}(Ho), was calculated from the temperature variation of the fitted magnitude of the ordered Ho moments, with the results shown in table 2. Figure 3 illustrates a fit of the model for Gd_{10}/Ho_{30} at $T = 12$ K. The estimates for each sample of the magnitude of the ordered Gd and Ho moments at this temperature are given in table 2, and are comparable with the bulk saturation moments [18] of $7.0\mu_{\mathrm{B}}$ and $10.0\mu_{\mathrm{B}}$, respectively. The fitted values for ϕ_{Ho} (both above and below T_{N}(Ho)) were found to agree to within $\pm 1.5^\circ$ with the initial values deduced from the total turn angles per bilayer, Φ (figure 1), and figure 4 shows the fitted values for ϕ_{Ho} in comparison to the values for a 5000 Å film of Ho grown on an Y seed [19].

After allowing for instrumental resolution, the widths of the fits of the model to the magnetic-scattering results from scans of $\boldsymbol{Q}$ along $[00\ell]$ were used to deduce the coherence lengths of the magnetic structures in the growth direction. The coherence lengths range from three to seven bilayers, as shown in figure 5, and are compared to those obtained from Tb/Ho [9] superlattices.

5. Discussion

The temperatures listed in table 2 for the onset of the ferromagnetic ordering of the Gd moments in the Gd/Ho superlattices are higher than the value for bulk Gd of T_{C}(Gd) $\approx$ 292 K. This enhancement may be related to the basal-plane compression of Gd imposed by the juxtaposition with Ho which has a smaller a lattice parameter. Table 2 lists the a

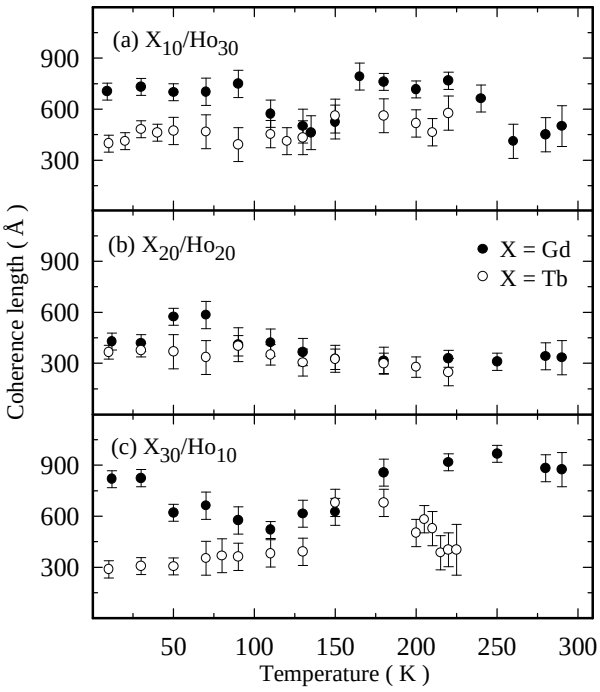

Figure 5. The temperature variations of the (resolution-corrected) coherence lengths of the magnetic structures in the growth direction for (a) X_{10}/Ho_{30}, (b) X_{20}/Ho_{20}, and (c) X_{30}/Ho_{10}, where for the solid points X = Gd, and for the open points X = Tb.

lattice parameters measured using neutrons at $T = 300$ K, which are smaller than the value for bulk Gd of 3.6360 [10]. An enhancement of T_C(Dy) was also reported for Dy/Lu [20] superlattices, for which the a lattice parameter of Lu is smaller than that of Dy.

The antiferromagnetic coupling above T_N(Ho) of adjacent Gd blocks within which moments are ferromagnetically aligned in the basal plane is consistent with the interactions between the Gd blocks being dominated by magnetic dipolar forces. These forces tend to cause a break-up of the macroscopic ferromagnetic order into domains. Above T_N(Ho), it is energetically favourable for the domain walls to lie in the nonmagnetic Ho blocks, and for the Gd moments to be aligned in the plane of the domain walls which is in the basal plane. Similar structures have been found for Dy/Lu [20] superlattices above T_N(Dy) and Tb/Ho [9] above T_N(Ho). In contrast, for Gd/Y [4] superlattices with $n_Y \lesssim 20$, the alignment between adjacent Gd blocks (within which moments were ferromagnetically aligned) was reported to oscillate between ferromagnetic and antiferromagnetic as n_Y was varied. The differences in the behaviour may arise because for Gd/Y superlattices RKKY interactions dominate the dipolar interactions, whereas for Gd/Ho, Tb/Ho, and Dy/Lu superlattices it is the dipolar interactions that dominate. A possible explanation is that the peak in the conduction-electron susceptibility for Y is larger and sharper than those for Ho or Lu [21], so the RKKY interactions can be expected to be stronger for superlattices with Y as a constituent. Gd/Dy [6, 22] superlattices were also reported to exhibit both antiferromagnetic and ferromagnetic structures above T_N(Dy), but it is less clear whether there was a simple correlation with the thickness of the Dy blocks. Further experiments on this system would be useful to clarify the results.

Below T_N(Ho), the temperature dependences of ϕ_{Ho} for the Gd/Ho superlattices are very similar to that of a 5000 Å thin film of Ho grown on an Y seed [19] (see figure 4). Such a similarity between the temperature dependences of ϕ_{Ho} for Ho-based superlattices and Ho thin films was reported for Ho/Pr [23] and Ho/Sc [15]. It was suggested that for these superlattices the conduction electrons of importance for the magnetism were largely confined to individual Ho blocks, in contrast to the situation for, for example, Ho/Y [16], Dy/Y [24], and Ho/Lu [21] superlattices. Given this interpretation, it would be reasonable to assume that for Gd/Ho superlattices nearest-neighbour exchange interactions are important for the propagation of magnetic order.

ϕ_{Ho} for the Gd/Ho superlattices varies smoothly with temperature unlike the case for Tb/Ho superlattices. This difference arises because in contrast to the small residual anisotropy for Gd, the basal-plane crystal-field anisotropy for Tb is much larger than for Ho, so for the Tb/Ho superlattices the total turn angle between successive ferromagnetic Tb blocks is approximately $m\pi/3$ (where m is an integer) which restricts the possible values of ϕ_{Ho} [9]. At very low temperatures $\phi_{Ho} \approx 36^\circ$, or equivalently $\boldsymbol{q} = (1/5)\boldsymbol{c}^*$, for all three Gd/Ho samples. This value is commensurate with the crystal lattice, and can be associated with the (221) spin-slip structure [25] (where 1 and 2 refer to the number of moments aligned along successive easy axes in the basal plane). The formation of spin-slip structures in Ho has been reported in several studies of MBE-grown rare-earth superlattices [15, 21] and thin films of Ho [19].

As seen from figure 5, the coherence lengths of the magnetic structure in Gd/Ho superlattices are comparable to those in Tb/Ho [9] superlattices. The possibly shorter coherence lengths for the magnetic structures in Tb/Ho superlattices at low temperatures may be related to the competition between the crystal-field basal-plane anisotropy of Tb and the indirect-exchange interaction. The lower coherence lengths at temperature above $T \approx 200$ K in Tb_{30}/Ho_{10} are associated with a mixed helical and ferromagnetic ordering in the Tb layers.

To conclude, the magnetic properties of Gd/Ho superlattices have been determined by neutron-diffraction techniques. Good fits to the magnetic-scattering results are obtained using a model that simulates the magnetic scattering from a ferromagnetic ordering of Gd moments with a helical ordering of Ho moments, with both the Gd and Ho moments confined to the basal plane at all temperatures measured. The coherence lengths of the magnetic structures range from three to seven bilayers. The results are consistent with those from previous studies of heavy rare-earth superlattices.

Acknowledgments

We would like to thank R A Cowley for his advice, and to acknowledge the expert assistance of the technical staff at Risø. The work in Oxford was funded by the EPSRC, and the experiments at Risø by the EU. CB-J is grateful for the award of an EPSRC studentship.

References

[1] Flynn C P and Salamon M B 1996 *Handbook of the Physics and Chemistry of the Rare Earths* vol 22, ed K A Gschneidner Jr and L Eyring (Amsterdam: Elsevier Science)
[2] Majkrzak C F, Kwo J, Hong M, Yafet Y, Gibbs D, Chien C L and Bohr J 1991 *Adv. Phys.* **40** 99
[3] Cowley R A, McMorrow D F, Swaddling P P, Ward R C C and Wells M R 1995 *Indian J. Pure Appl. Phys.* **33** 509
[4] Majkrzak C F, Cable J W, Kwo J, Hong M, McWhan D B, Yafet Y, Waszczak J V and Vettier C 1986 *Phys. Rev. Lett.* **56** 2700

[5] Yafet Y 1987 *J. Appl. Phys.* **61** 4058
[6] Majkrzak C F, Gibbs D, Böni P, Goldman A I, Kwo J, Hong M, Hsieh T C, Fleming R M, McWhan D B, Yafet Y, Cable J W, Bohr J, Grimm H and Chien C L 1988 *J. Appl. Phys.* **63** 3447
[7] Simpson J A, Cowley R A, Jehan D A, Ward R C C, Wells M R, McMorrow D F, Clausen K N, Thurston T R and Gibbs D 1996 *Z. Phys.* B **101** 35
[8] Simpson J A, Cowley R A, McMorrow D F, Ward R C C, Wells M R, Carlile C J and Adams M A 1996 *J. Phys. C: Solid State Phys.* **8** L187
[9] Bryn-Jacobsen C, Cowley R A, McMorrow D F, Goff J P, Ward R C C and Wells M R 1997 *Phys. Rev.* B **55** 14 360
[10] Wyckoff R W G 1965 *Crystal Structures* vol 1 (New York: Interscience)
[11] Corner W D and Tanner B K 1976 *J. Phys. C: Solid State Phys.* **9** 627
[12] Will G, Nathans R and Alperin H A 1994 *J. Appl. Phys.* **35** 1045
[13] Koehler W C, Cable J W, Wilkinson M K and Wollan F O 1966 *Phys. Rev.* **151** 414
[14] Ward R C C and Wells M R 1997 *Proc. of Joint UK Magnetism Workshop (Dublin)*
[15] Bryn-Jacobsen C, Cowley R A, McMorrow D F, Goff J P, Ward R C C and Wells M R 1997 *Phys. Rev.* B **55** 317
[16] Jehan D A, McMorrow D F, Cowley R A, Ward R C C, Wells M R, Hagmann N and Clausen K N 1993 *Phys. Rev.* B **48** 5594
[17] Squires G L 1978 *Introduction to the Theory of Thermal Neutron Scattering* (Cambridge: Cambridge University Press)
[18] Jensen J and Mackintosh A R 1991 *Rare Earth Magnetism—Structures and Excitations* (New York: Oxford Science)
[19] Cowley R A, Ward R C C, Wells M R, Matsuda M and Sternlieb B 1994 *J. Phys. C: Solid State Phys.* **6** 2985
[20] Beach R S, Borchers J A, Matheny A, Erwin R W, Salamon M B, Everitt B, Pettit K, Rhyne J J and Flynn C P 1993 *Phys. Rev. Lett.* **70** 3502
[21] Swaddling P P, Cowley R A, Ward R C C, Wells M R and McMorrow D F 1996 *Phys. Rev.* B **53** 6488
[22] Camley R E, Kwo J, Hong M and Chien C L 1990 *Phys. Rev. Lett.* **64** 2703
[23] Simpson J A, McMorrow D F, Cowley R A, Wells M R and Ward R C C 1995 *J. Phys. C: Solid State Phys.* **7** L417
[24] Salamon M B, Borchers J, Sinha S, Du R, Cunningham J E and Flynn C P 1987 *Phys. Rev.* B **35** 6808
[25] Cowley R A and Bates S 1988 *J. Phys. C: Solid State Phys.* **21** 4113